# Observation of the Photorefractive Effect in a Hybrid Organic−Inorganic Nanocomposite

**Jeffrey G. Winiarz, Liangmin Zhang, Manjari Lal, Christopher S. Friend, and Paras N. Prasad***

*Contribution from the Photonics Research Laboratory, Departments of Chemistry and Physics, State University of New York at Buffalo, Buffalo, New York 14260*

*Received October 8, 1998. Revised Manuscript Received March 31, 1999*

**Abstract:** We report the observation of the photorefractive effect in an organic−inorganic polymer composite photosensitized with nanosized cadmium sulfide particles, the surface of which is passivated utilizing *p*-thiocresol. The semiconductor nanoparticles are dispersed in a poly(*N*-vinylcarbazole) (PVK) polymer matrix that also acts as the charge-transport species. The ability of these particles to behave as the photosensitizer in a PVK matrix has been characterized through a dc photoconductivity experiment. In addition, for the photorefractive experiments, the second-order optically nonlinear chromophore 4-nitrophenyl-L-prolinol is also doped into the PVK matrix to elicit electro-optic response. Tricresyl phosphate is used to lower the glass-transition temperature of the material, allowing for room temperature in situ poling of the sample. In addition to the electric field dependence of the degenerate four-wave mixing diffraction efficiency, the photorefractive nature of the grating is confirmed via two-wave mixing asymmetric energy transfer. The paper also discusses briefly the methods employed in the syntheses of the capped CdS nanoparticles used in this study, which include the reverse micelle approach as well as competitive reaction chemistry. The resulting particles have been characterized using UV−vis absorption and X-ray diffraction.

## Introduction

The realization of advanced information and image processing technology depends on the development of multifunctional materials which are able to simultaneously satisfy several requirements.[1,2] Semiconductor nanoparticles, which exhibit properties different from the bulk materials, are a new class of materials which hold considerable promise for numerous applications in the fields of electronics and photonics. Nanoscale modification of molecular design and morphology of such particles provides a powerful approach to control their electronic and optical properties as well as their processability. These properties include quantum size effect on photoreactivity[3] and photocatalytic activity as well as their applications in nonlinear optics.[4−11]

The physical properties of semiconductor nanocrystallites are dominated by quantum confinement, the widening HOMO−LUMO gap with decreasing particle size which directly affects the photophysics of the material. Due to this fact, the proper control of particle size is critical in any investigation involving these materials. Typically, nuclei of a desired material are grown to the required size and then passivated by one of many possible organic molecules. Alternatively, agglomeration of the clusters can be prevented by entrapment of the particles in a rigid media such as polymers or zeolites.[12,13] In the current investigation, the surface of the nanocrystallites has been capped through the covalent addition of thiols, which serve not only as a source of sulfide ions but also as growth moderators.[14] This property stems from the ability of the thiolate ions to bind to cadmium ions in the 1+ oxidation state located at the particle surface, thereby effectively inhibiting further growth of the CdS particles.[15,16]

Semiconductor clusters are a potentially useful class of polymer photosensitizers in many applications that require materials with photoconductive and photorefractive properties. While there are several polymers known which show reasonable charge generation in the ultraviolet region, it is often desirable to enhance their optical response in the visible portion of the spectrum. Since only a small amount of nanoclusters are required (typically a few weight percent) to photosensitize the matrix, the nanoclusters are isolated from each other and are responsible for the charge generation while the polymer is responsible for charge transport.[17,18] Although not much work has been done

(1) Klein, L. C., Ed. *Photonics and Nonlinear Optics with Sol−Gel Processed Inorganic Glass: Organic Polymer Composite*; Kluwer Academic: Boston, 1994; Chapter 19.
(2) Mark, J. E., Lee, C. Y. C., Bianoni, P. A., Eds. *Hybrid Organic−Inorganic Composites*; ACS Symposium Series 585; American Chemical Society: Washington, DC, 1995; Chapter 25.
(3) Wang, Y.; Suna, A.; Mchugh, J. *J. Chem. Phys.* **1990**, *92*, 6927−6939.
(4) Brus, L. E. *J. Chem. Phys.* **1983**, *79*, 5566−5571.
(5) Rosetti, R.; Hull, R.; Gibson, J. M.; Brus, L. E. *J. Chem. Phys.* **1985**, *82*, 552−559.
(6) Alivisatos, A. P.; Harris, A. L.; Levinos, N. J.; Steigerwald, M. L.; Brus, L. E. *J. Chem. Phys.* **1988**, *89*, 4001−4011.
(7) Alivisatos, A. P. *Science* **1996**, *271*, 933−937.
(8) Herron, N.; Wang, Y.; Eckert, H. *J. Am. Chem. Soc.* **1990**, *112*, 1322−1326.
(9) Tobin, J. G.; Colvin, V. L.; Alivisatos, A. P. *J. Vac. Sci. Technol.* **1991**, *A9*, 852−853.
(10) Brus, L. E. *J. Chem. Phys.* **1984**, *80*, 4403−4409.
(11) Wang, Y.; Herron, N. *J. Phys. Chem.* **1991**, *95*, 525−532.
(12) Hilinski, E.; Lucas, P.; Wang, Y. *J. Chem. Phys.* **1988**, *89*, 3435−3441.
(13) Wang, Y.; Herron, N. *J. Phys. Chem.* **1987**, *91*, 257−260.
(14) Nosaka, Y.; Yamaguchi, K.; Miyama, H.; Hayashi, H. *Chem. Lett.* **1988**, 605−608.
(15) Swayambunathan, V.; Hayes, D.; Schmidt, H. K.; Liao, Y. X.; Meisel, D. *J. Am. Chem. Soc.* **1990**, *112*, 3831−3837.
(16) Kundu, A.; Khosravi, A. A.; Kulkarni, S. K. *J. Mater. Sci.* **1997**, *32*, 245−258.
(17) Wang, Y.; Herron, N. *Chem. Phys. Lett.***1992**, *200*, 71−75.

10.1021/ja983559w CCC: $18.00 
Published on Web 05/18/1999

in this direction, previously reported results have indicated very low photocharge generation efficiency of the polymers which may be explained by the lack of ability to achieve sufficiently high loading of the semiconductor clusters.[17] In this paper, we report enhanced photoconductivity of a poly(*N*-vinylcarbazole) (PVK):CdS system and enhanced two-beam coupling and diffraction efficiency of a CdS:PVK:TCP:NPP (TCP = tricresyl phosphate, NPP = 4-nitrophenyl-L-prolinol) system which may be due to an increased solubility of CdS clusters in the polymer matrix. This enhanced solubility is achieved through encapsulation of the CdS particles in an organic coating of the capping reagent thiocresol, thereby making the surface hydrophobic. Also, capping of the CdS particles prevents secondary growth, enabling the particles to maintain their size.[15,16]

The methods used in the synthesis of the CdS particles can be divided into two main categories: (i) one in which the eventual size of the particle is controlled by adjusting the ratio of sulfide to thiolate, taking advantage of the competitive reaction rate of these species with cadmium ions, and (ii) the second method in which ultimate cluster size is dictated by the size of a reverse micelle inside which the particle is grown. In the first method, described as competitive reaction chemistry (CRC),[8] the mechanism of cluster formation has been termed as an inorganic form of polymerization. In the initiation phase of the synthesis a solution containing cadmium ions generated from cadmium acetate is introduced into a solution containing $S^{2-}$ and $RS^{-}$, in the form of sodium sulfide and *p*-thiocresol, respectively, to create small particles of CdS. Once formed, a propagation step in which the particles aggregate competes with the growth-terminating reaction of the thiolate with the surface of the particle.[8] It has also been shown that, although being covalently bonded to the surface of CdS particles, the thiocresol species is dislocated by additional sulfide ions allowing for further growth of the cluster. However, once a sulfide ion has been incorporated into a given cluster, it cannot be replaced by a thiolate ion.[8] Through this process the particles are allowed to grow until the supply of $S^{2-}$ has been exhausted.

The second method involves the use of reverse micelles (RMs) as microreactors to obtain organically encapsulated nanoparticles. The reverse micellar system is generally composed of two immiscible liquids (water and oil) where the aqueous phase is dispersed as nanosize water droplets encapsulated by a monolayer film of surfactant molecules in a continuous nonpolar organic solvent such as a hydrocarbon. In this study the continuous oil phase consists of isooctane and sodium bis(2-ethylhexyl)sulfosuccinate (AOT) serves as the surfactant. In addition to water, aqueous solutions containing a variety of dissolved salts, including cadmium acetate and sodium sulfide, can be solubilized within the reverse micelles.[19] The size of the micelle, and subsequently the volume of the aqueous pool contained within the micelle, is governed by the water-to-surfactant ratio, also termed $W_0$, where $W_0 = [H_2O]/[\text{surfactant}]$.[20] Continuous exchange of the micellar contents through dynamic collisions enables the reaction to proceed; however, since the reaction is confined within the cavity of the micelle, growth of the particle beyond the dimensions of the cavity is inhibited. In the final stage of this synthesis, the passivating reagent, *p*-thiocresol, is added to the continuous oil phase. This species is then able to enter the aqueous phase as $RS^{-}$ and bond to the surface of the contained particle, eventually rendering the surface of the particle hydrophobic, inducing precipitation of the capped CdS.

Both methods of particle preparation presented yield a free-flowing powder which is stable for several weeks at ambient conditions allowing for X-ray diffraction (XRD) characterization of the product. The powders are easily redispersed in several organic solvents such as pyridine, dimethylformamide, and cyclopentanone, allowing for optical characterization of the solvated product as well as doping of a polymer (PVK) matrix to form an inorganic:organic composite system. Since all the particles used in this study had diameters less than 22 Å (determined via XRD), optical scattering was not observed, permitting their use in optical applications (e.g., photorefractivity).

Photorefractivity in polymeric systems, considered to be potential media for high-density optical data storage, optical amplification, and dynamic image processing, is an area of considerable recent interest where major achievements have been made.[21−27] The phenomenon of photorefractivity in polymeric composites can be realized in materials which simultaneously exhibit photoconductive and electro-optic (EO) properties.[28,29] It should be noted that, while these properties are necessary for the observation of the photorefractive effect, their presence does not necessarily imply that a particular material will possess photorefractive properties. Photoconductivity allows for the formation of an internal space-charge electric field through a subsequent combination of photogeneration, transport, and trapping of charge carriers. Electro-optic response by the same material results in the modulation of the material's refractive index through a Pockels effect as a result of the periodic space-charge field. The resulting manifestation of these processes is a light-induced phase grating (hologram). Photorefractive holograms are generated in the form of a refractive index grating written by the interference pattern generated when two laser beams are crossed in the medium which can then be retrieved through the diffraction of a probe beam.[21,24,25,30,31]

An unusual feature of the photorefractive grating is the phase shift between the intensity pattern (intensity of the overlapped beams) and the resulting periodic refractive index modulation. This phenomenon gives rise to asymmetric energy transfer in two-beam coupling experiments wherein one beam gains intensity at the expense of the other.

In this paper, we report some of the typical photorefractive figures of merit, that is, steady-state diffraction efficiency ($\eta_{ss}$) and two-wave mixing gain coefficient ($\Gamma$) for the PVK:TCP:NPP composite photosensitized with nanoparticles of the inorganic semiconductor, CdS.

(18) Wang, Y. *Pure Appl. Chem.* **1996**, *68*, 1475−1478.
(19) Masui, T.; Fujiwara, K.; Machida, K.; Adachi, G.; Sakata, T.; Mori, H. *Chem. Mater.* **1997**, *9*, 2197−2204.
(20) Pileni, M. P. *J. Phys. Chem.* **1993**, *97*, 6961−6973.
(21) Moerner, W. E.; Silence, S. M. *Chem. Rev.* **1994**, *94*, 127−155.
(22) Kippelen, B.; Marder, S. R.; Hendrickx, E.; Maldonado, J. L.; Guillemet, G.; Volodin, B. L.; Steele, D. D.; Sandalphon, Y. Enami; Yao, Y. J.; Wang, J. F.; Rockel, H.; Erskine, L.; Peyghambarian, N. *Science (Washington, D.C.)* **1998**, *279*, 54−57.
(23) Hendrickx, E.; Herlocker, J.; Maldonado, J. L.; Guillemet, G.; Rockel, H.; Erskine, L.; Marder, S. R.; Kippelen, B.; Peyghambarian, N. *Proc. SPIE−Int. Soc. Opt. Eng.* **1998**, *3281*, 268−276.
(24) Prasad, P. N.; Cui, Y.; Swedek, B.; Cheng, N.; Kim, K. S. *J. Phys. Chem. B.* **1997**, *101*, 3530−3534.
(25) Zhang, Y.; Burzynski, R.; Ghoshal, S.; Casstevens, M. K. *Adv. Mater.* **1996**, 8, 111−125.
(26) Wang, Q.; Gharavi, A.; Li, W.; Yu, L. *Polym. Prepr. (Am. Chem. Soc., Div. Polym. Chem.)* **1997**, *38*, 516−517.
(27) Peng, Z.; Gharavi, A. R.; Yu, L. *J. Am. Chem. Soc.* **1997**, *119*, 4622−4632.
(28) Gunter, P.; Huignard, J. P., Eds. *Photorefractive Materials and Their Applications*; Springer-Verlag: Berlin, 1988; I & II, Topics in Applied Physics, Vols. 61 and 62.
(29) Yeh, P. *Introduction to Photorefractive Nonlinear Optics*; Wiley: New York, 1993.

## Experimental Section

**Materials.** Sodium bis(2-ethylhexyl)sulfosuccinate, *n*-heptane, *p*-thiocresol, cadmium acetate dihydrate, sodium sulfide, poly(vinylcarbazole), tricresyl phosphate, pyridine, methanol, and acetonitrile were obtained from Aldrich at the highest purity available and used without further purification. The nonlinear dye 4-nitrophenyl-L-prolinol was obtained from Laser Photonics Technology, Inc.

**CRC Preparation of Organically Encapsulated CdS.** This synthesis is based on that described in the literature[8] with minor modifications described here. The sulfide to *p*-thiocresol ratios used in this method of CdS preparation were $S^{2-}$:$RS^-$ = 1:2, 1:1, 1:0.2, 1:0.1, 1:0.02. With the exception of *p*-thiocresol concentration, which was adjusted to achieve the desired sulfide to *p*-thiocresol ratio, all parameters were held constant. The following represents a typical synthesis ($S^{2-}$:$RS^-$ = 1:0.2).

Sodium sulfide (0.8 g, 10 mmol) and *p*-thiocresol (0.25 g, 2 mmol) were dissolved in 50 mL of water, 50 mL of methanol, and 100 mL of acetonitrile, vigorously stirred, and purged with nitrogen for 15 min. To this solution was added dropwise cadmium acetate dihydrate (5.34 g, 20 mmol) dissolved in a mixture of methanol (160 mL) and acetonitrile (40 mL), yielding an opaque orange dispersion. This dispersion was evaporated to dryness, and the product was washed exhaustively with methanol, yielding a free-flowing yellow powder.

**Reverse Micelle Preparation of Organically Encapsulated CdS.** For this method of preparation, CdS clusters were prepared with $W_0$ = 10, 15, and 20. Here, all parameters were held constant with the exception of water concentration, which was adjusted to achieve the desired $W_0$. For $W_0$ = 10 the procedure is as follows.

Two solutions of sodium bis(2-ethylhexyl)sulfosuccinate (8.9 g, 20 mmol) in 200 mL of *n*-heptane were prepared. To one of these solutions was added cadmium acetate dihydrate (96 mg, 0.36 mmol) in 3.6 mL of water, and to the other was added sodium sulfide (28 mg, 0.36 mmol) in 3.6 mL of water. These two solutions were simultaneously poured into a single vessel producing a nonscattering yellow dispersion, followed by the immediate introduction of *p*-thiocresol (0.28 g, 3.6 mmol) in 36 mL of heptane. After stirring the reaction mixture for 24 h, the precipitated surface capped CdS was collected and washed with methanol, yielding a free-flowing powder.

**Samples for Photoconductivity Measurements.** The main goal of the photoconductivity experiments was to determine which method of CdS preparation afforded the most efficient PVK sensitizer. For this reason TCP and NPP were not added to these samples. Pyridine was used to first dissolve the CdS followed by the introduction of PVK, affording a sample with a PVK:CdS ratio of 100:1 by weight. This mixture was subjected to ultrasound "mixing" until a homogeneous dispersion was obtained. It was filtered through a 0.2 $\mu$m pore size membrane and used for film fabrication. Thin films (3−5 $\mu$m) were fabricated via conventional spin-coating techniques on a glass substrate coated with indium tin oxide (ITO). The film thickness as well as the surface integrity of the film surface were confirmed using a Tencor Alpha-step 500 surface profilometer. Counter electrodes (diameter = 5 mm) were fabricated on the polymer surface through high-vacuum deposition of silver which could be physically contacted. Photoconductivity measurements were made using a simple dc photocurrent technique where a dc voltage is applied to the sample and the current component induced by light excitation is measured.[32] In addition to thermal grounding of the sample via an aluminum block, the photoconductivity experiment was repeated with the black paint applied to the substrate, under which conditions no appreciable increase of the dark current was observed.

**Samples for Photorefractivity Measurements.** Similar to the photoconductivity samples, CdS was first dissolved in pyridine followed by the subsequent introduction of PVK, TCP, and NPP, where the weight percent composition of PVK:TCP:CdS:NPP is represented by the ratio 56.5:37.5:0.191:5.74. The filtered dispersion (0.2 $\mu$m pore size membrane) was cast on ITO-coated glass substrates with an etched electrode pattern. The films were allowed to dry at ambient conditions for 24 h and subsequently heated to 70 °C in a vacuum oven for 24 h to ensure complete solvent evaporation. Next, two films were softened by placing them on a hot plate (200 °C) for 30 s and pressed together to produce a sandwich glass−ITO−polymer−ITO−glass arrangement between the etched ITO-coated substrates, yielding samples which were 100−200 $\mu$m in thickness. The glass transition temperature ($T_g$) of the composite was determined to fall below 14 °C, the lower detection limit of the employed differential scanning calorimeter. The film preparation was performed in a class 100 cleanroom.

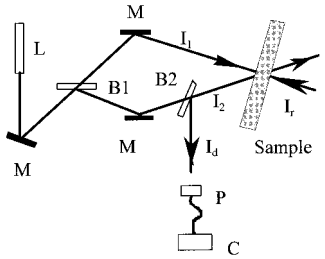


**Figure 1.** Schematic of the experimental setup for two-wave mixing and four wave mixing: $I_1$ and $I_2$, writing beams; $I_r$, reading beam; $I_d$, diffracted beam; L, argon ion laser; B, beam splitter; M, mirror; C, computer; P, photodetector.

The photorefractive properties of the PVK:NPP:TCP:CdS composite samples were studied via two-wave mixing (TWM) and degenerate four-wave mixing (DFWM) techniques using an oblique experimental setup described by Figure 1. Holographic gratings were written through the intersection of two coherent beams generated by an $Ar^+$ laser operating at 514.5 nm with s-polarization in the four-wave mixing (FWM) experiment and p-polarization in the TWM experiment. The two writing beams, $I_1$ and $I_2$, intersected in the sample with incident angles of $\theta_1$ = 60° and $\theta_2$ = 38° (in air), respectively, creating an intensity grating with a grating spacing, $\Lambda$, of 1.85 $\mu$m. In the DFWM experiment, a p-polarized reading beam ($I_r$) propagated in a direction opposite of one of the writing beams ($I_1$). In the TWM experiments, the asymmetric energy transfer between the p-polarized writing beams was observed by monitoring the intensity of each of the writing beams by two photodetectors (not depicted in Figure 1) when an external electric field was applied. All data were digitized using a digital multimeter and transferred to a computer. For steady-state conditions, the data were collected for a period of 30 s and averaged.

The UV−vis absorption spectra were recorded on a Shimadzu UV-3101 spectrophotometer. UV−vis spectra were obtained using a dispersion of 4 mg of capped CdS in 5.0 g of pyridine in a 1 cm thick quartz cell except where otherwise noted.

The electro-optic properties of the composite were measured using the transmission configuration of the ellipsometric technique[33] as well as a conventional Mach−Zender interferometric setup.[30,34,35] Both versions of this experiment were performed with samples identical to those used in making photorefractive characterizations, thus eliminating unwanted interference caused by multiple beam reflections commonly associated with thinner films, which often leads to inaccurate assessment of the electro-optic coefficients.[36] For the Mach−Zender interferometric measurements a poling voltage of 54 V/$\mu$m was applied to the sample as well as an ac modulating field of ~1 V/$\mu$m.

## Results and Discussion

In Figure 2a, the absorption spectra of representative ($W_0$ = 10 and 20) thiocresol-encapsulated CdS nanoparticles, as prepared using RM techniques, are presented. The absorption spectra of these particles clearly show the blue shift associated

(30) Swedek, B.; Cheng, N.; Cui, Y.; Zieba, J.; Winiarz, J.; Prasad, P. N. *J. Appl. Phys.* **1997**, *82*, 5923−5931.
(31) Ducharme, S.; Scott, J. C.; Twieg, R. J.; Moerner, W. E. *Phys. Rev. Lett.* **1991**, *66*, 1846−1849.
(32) Schildkraut, J. S. *Appl. Phys. Lett.* **1991**, *58*, 340−342.
(33) Teng, C. C.; Man, H. T. *Appl. Phys. Lett.* **1990**, *56*, 1734−1736.
(34) Sigelle, M.; Hierle, R. *J. Appl. Phys.* **1981**, *52*, 4199.
(35) Singer, K. D.; Kuzyk, M. G.; Holland, W. R.; Sohn, J. E.; Lalama, S. L.; Comizzoli, R. B.; Katz, H. E.; Schilling, M. L. *Appl. Phys. Lett.* **1996**, *53*, 1800.
(36) Schildkraut, J. S. *Appl. Opt.* **1990**, *29*, 2839−2841.

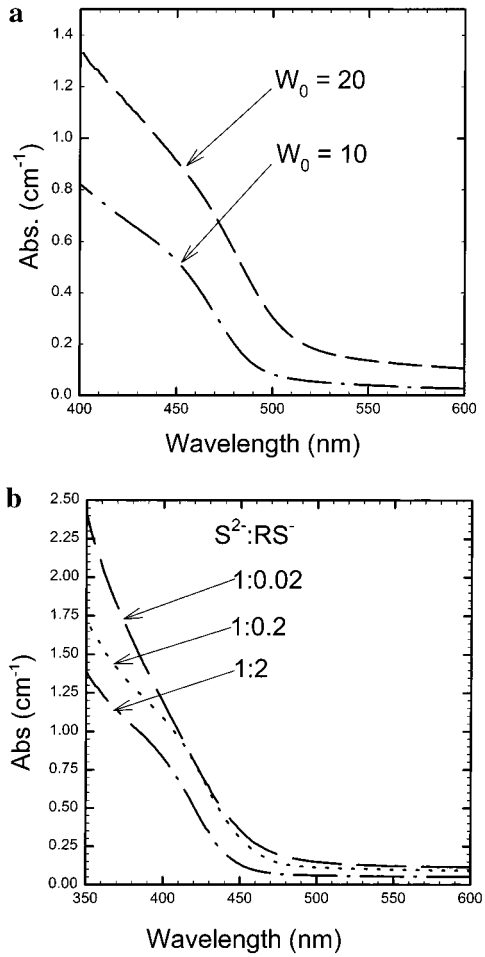


**Figure 2.** UV−visible absorption spectra for surface passivated CdS prepared using (a) RM techniques ($W_0$ = 10 and 20) and (b) CRC techniques ($S^{2-}$:$RS^-$ = 1:2, 1:0.2, and 1:0.02).

with the quantum confinement effects commonly observed in nanosize clusters. Compared with bulk CdS (not shown), which possesses an absorption shoulder at 512 nm, CdS prepared with $W_0$ = 20 possesses an absorption shoulder which has been shifted to 465 nm, and those prepared under the conditions of $W_0$ = 10, representing a smaller droplet size, are further shifted to 455 nm. This shift in the band-gap demonstrates the ability to control the optical properties of the final product through the appropriate choice of $W_0$.

Similarly, encapsulated CdS prepared using CRC techniques, the spectra of which are presented in Figure 2b for $S^{2-}$:$RS^-$ = 1:2, 1:0.2 and 1:0.02, exhibit the same shift toward the blue. In this example it is noticed that, as the relative amount of passivating reagent is increased, the observed shift becomes more pronounced. As was the case with the CdS nanoparticles prepared by reverse micelle techniques, a convenient means of controlling a material's optical properties is realized.

To confirm that the blue shift observed in these samples was accompanied by the expected reduction in average size, size determination was conducted through XRD in conjunction with the Scherrer formula

$$d = 0.9\lambda/(\beta \cos 2\theta) \qquad (1)$$

where $\lambda$ is the wavelength of the scanning radiation, $\beta$ is the full width at half-maximum of the peak in question, and $\theta$ is the angle at which the peak is centered.[37] This formula

(37) Taylor, A. *X-Ray Metallography*; Wiley: New York, 1961.

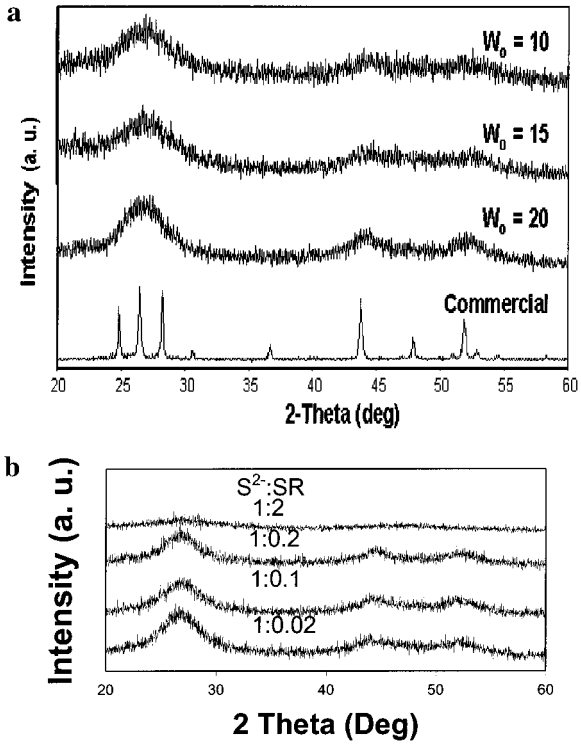


**Figure 3.** X-ray diffraction spectra for surface passivated CdS powder prepared using (a) RM techniques ($W_0$ = 10, 15, and 20) and (b) CRC ($S^{2-}$:$RS^-$ = 1:2, 1:0.2, 1:0.1, and 1:0.02).

quantitatively relates the observed broadening of X-ray diffraction lines with the finite size of the sphalerite crystalline particles. Using eq 1, it was calculated that the sizes of the particles are <14, 18, and 21 Å for $W_0$ = 10, 15, and 20, respectively (the XRD obtained for 5 $\mu$m commercial CdS powder is included for purposes of comparison), and for the nanoparticles synthesized using CRC techniques, the sizes of the particles are <14, 16, 18, and 22 Å for $S^{2-}$:$RS^-$ = 1:2, 1:0.2, 1:0.1, and 1:0.02, respectively (14 Å being the lower limit of the Sherrer formula) (Figure 3).

The photosensitivity $S_{ph}$ (photoconductivity per unit light intensity) of PVK doped with CdS prepared via RM methods ($W_0$ = 10) at excitation wavelengths of 514.5 and 488 nm is presented in Figure 4a and was calculated according to the following equation:

$$S_{ph} = \sigma/P = J_{ph}/EP \qquad (2)$$

where $\sigma$ is the photoconductivity, $J_{ph}$ is the photocurrent density, $E$ is the applied electric field, and $P$ is the illumination intensity of the beam. Enhanced photosensitivity is observed at 488 nm when compared with longer wavelengths due to the higher absorption cross section of the sensitizer at this wavelength. In Figure 4b the photosensitivity of CdS prepared by the same method but with varying $W_0$ is supplied at $\lambda$ = 514.5 nm. Here it is observed that the photoconductivity is greater for particles prepared at a droplet size of $W_0$ = 20. This is so because the CdS particles ($W_0$ = 10) are smaller in size than are those prepared using $W_0$ = 20, and the absorption edge is further blue-shifted from the operating wavelength, resulting in a diminished absorption cross section and a decrease in photosensitivity.

The photosensitivity at 514.5 nm of encapsulated CdS prepared by the CRC method with various $S^{2-}$:$RS^-$ ratios is depicted in Figure 5. It was observed that the photosensitivity of the CdS:PVK composite increased as the relative amount of capping reagent was decreased until the ratio of 1:0.2 was

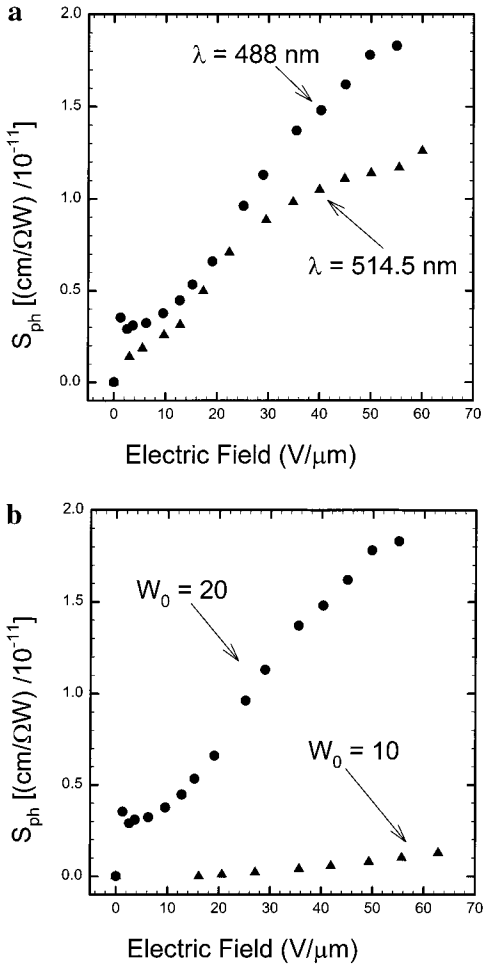


**Figure 4.** Photosensitivity $S_{ph}$ versus electric field of CdS prepared using RM techniques in PVK (a) at 488 nm (circles) and 514.5 nm (triangles) where $W_0 = 10$ and (b) at 514 nm where $W_0 = 10$ (triangles) and 20 (circles).

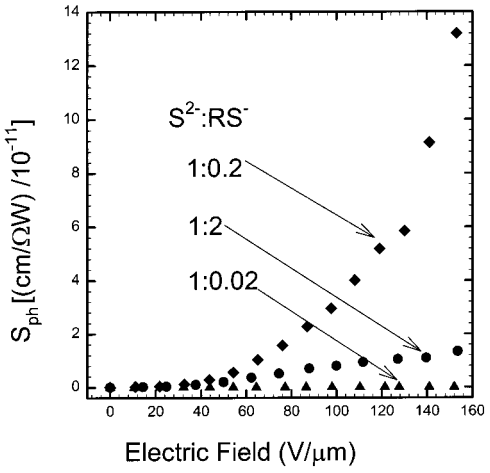


**Figure 5.** Photosensitivity $S_{ph}$ versus electric field at 514.5 nm for CdS prepared using CRC techniques in PVK for $S^{2-}$:$RS^-$ = 1:2 (circles), 1:0.2 (diamonds), and 1:0.02 (triangles).

reached, at which point the particles became almost insoluble in solvents compatible with PVK. The explanation for this trend in observed photosensitivity lies in the fact that, as the relative concentration of capping reagent is decreased, the average cluster size is increased, which implies a decrease in the magnitude of the observed blue shift in the absorption spectrum. Since smaller particles possess a diminished absorption cross

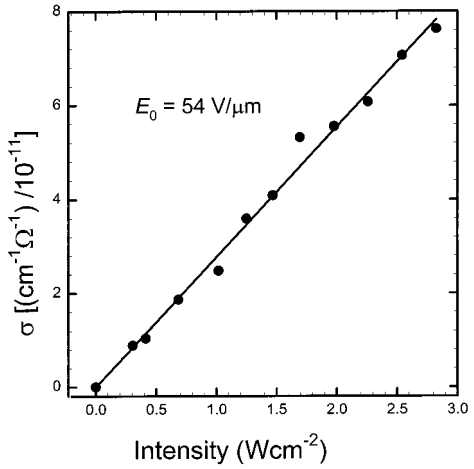


**Figure 6.** Photoconductivity $\sigma$ versus illumination intensity $I_I$ at 514.5 nm for PVK:CdS ($S^{2-}$:$RS^-$ = 1:0.2). The line represents a linear least-squares fit of the data.

section at 514.5 nm, the photosensitizing nature of these clusters is also expected to be diminished.

On the basis of the results obtained in the photoconductivity study, it was determined that CdS prepared employing CRC techniques with a $S^{2-}$:$RS^-$ ratio of 1:0.2 would be utilized in the photorefractive portion of the study, and for the remainder of this paper, it will be assumed that it is this CdS which is referred to unless otherwise stated.

To determine if the phenomenon of bimolecular recombination was present in the photoconductive mechanism associated with this composite (PVK:CdS), the photoconductivity of the composite was determined as a function of illumination intensity ($I_I$). These data are presented in Figure 6 for $\lambda = 514.5$ nm with an applied electric field of 54 V/$\mu$m. As is evident, the photoconductivity is linearly dependent on $I_I$, suggesting the absence of bimolecular recombination which, if present, would cause the photoconductivity to exhibit an $I_I^2$ dependence. It is also noted that, for the aforementioned composite, the dark current density was approximately 0.05% of the photocurrent density.

Since the concentration of nanoclusters lies well below the percolation threshold, it is assumed that CdS acts mainly as a sensitizer and PVK is responsible for charge transport (positive charges in this case, as PVK is a well-established hole transporting polymer) in this composite.[17] On the basis of this knowledge, it can be assumed that the photoconductive mechanism is initiated with the absorption of a photon by a CdS cluster. This in turn gives rise to an electron−hole pair which is rapidly trapped on the surface of the particle. Given that the electron affinity of CdS nanocrystals exceeds that of PVK, the transfer of a hole from the nanoparticle to the polymer is energetically favorable. However, how charge transport is able to occur across the inert passivating layer is the subject of current debate.[38] In recent literature[39] several possibilities have been proposed, the first of which involves the tunneling of charge carriers through the passivating layer. This explanation is unlikely, since the probability of tunneling through such sizable barriers, as those represented by even a monolayer of capping molecules used in this study, is quite small. A second explanation offered by the same authors postulates that, despite the wide band gap nature of organic capping passivating molecules, if

(38) Greenham, N. C.; Xiaogang, P.; Alivisatos, A. P. *Phys. Rev.* **1996**, *54*, 17628−17637.

(39) Nanda, J.; Narayan, K. S.; Kuruvilla, B. A.; Murthy, G. L.; Sarma, D. D. *Appl. Phys. Lett.* **1998**, *72*, 1335−1337.

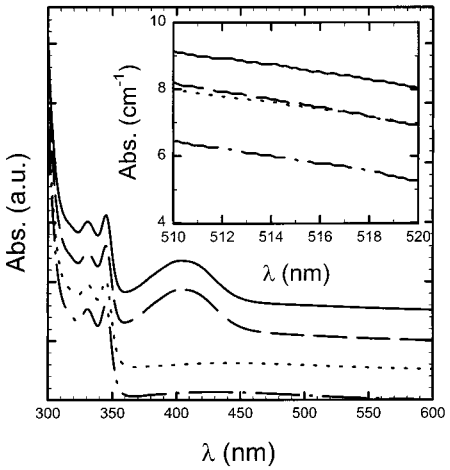


**Figure 7.** UV−visible absorption spectra for PVK:TCP (− · −), PVK:TCP:CdS (···), PVK:TCP:NPP (- - -), and PVK:TCP:NPP:CdS (—).

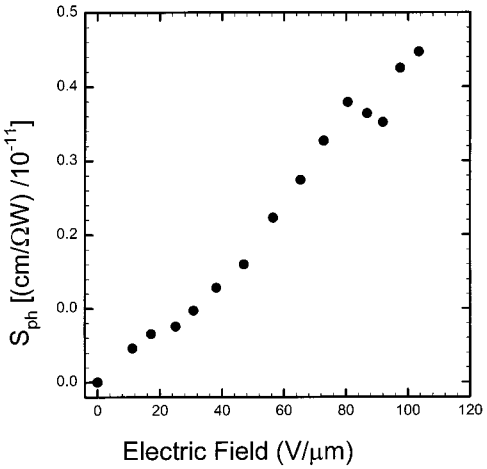


**Figure 8.** Photosensitivity $S_{ph}$ versus electric field at 514.5 nm for PVK:TCP:NPP:CdS.

the valence band of these molecules overlaps with that of CdS, it would be possible for the passivating layer to support charge transport.

Finally, it may be possible that the use of pyridine as a solvent provides a kinetic pathway by which CdS can complex with PVK, in which case the effects of the passivating layer can be essentially neglected. This hypothesis is based on observations reported in the literature.[17,38] First, it has been shown that pyridine is effective in the removal of organic capping ligands. This is due to the high affinity of the lone pair of electrons associated with the nitrogen atom for the surface of CdS nanoparticles.[17] Similarly, the ability of the amine group residing in the PVK molecule to complex with the surface of CdS particles has been established.[38] It may be possible that, upon sufficient removal of the thiocresol capping reagent by pyridine, PVK and pyridine enter into an equilibrium in which a portion of the CdS nanoclusters are complexed with PVK, which would promote the charge-transfer process. The lack of solubility exhibited by the CdS particles in alternative solvents complicates the confirmation of these speculations.

While various mechanisms of charge transfer between the charge-generating and the charge-transporting species in these hybrid materials have been proposed, it is almost certain that several mechanisms play a significant role in this process.[17] This observation is based on the variety of polymer−nanoparticle and nanoparticle systems exhibiting photoconductive properties, with the dominant mechanism seemingly depending on the nature of the material in question since a single mechanism could not possibly justify the magnitude of photoconductivity reported in each of these systems. The dominant characteristics of the charge-transfer process in this particular composite is the subject of current studies.

The UV−vis absorption characteristics of PVK:TCP, PVK:TCP:CdS, PVK:TCP:NPP, and PVK:TCP:CdS:NPP thin films were collected and are presented in Figure 7 (the spectra in the main figure, i.e. not the inset, have been offset by 50 cm$^{-1}$ with respect to each other for clarity). With the exception of sample composition, which was designed to match that of the photorefractive samples, the thin films used in these portions of the experiment were fabricated identically to photoconductive samples. For photorefractive applications it is ideal to fabricate a composite in which the sensitizer possesses the smallest band gap with respect to the other components.[21,25] This allows for operation at an optical wavelength which is preferentially absorbed by the photosensitizer, eliminating background absorption by the other components.[21,25] The absorption coefficient, $\alpha$, at 514.5 nm of PVK:TCP is increased from around 6.0 cm$^{-1}$ to approximately 7.6 cm$^{-1}$ as a result of the addition of CdS (see Figure 7). However, the addition of NPP also results in an increase in $\alpha$ to about 7.6 cm$^{-1}$. Finally, the inclusion of both NPP and CdS in the composite increases $\alpha$ to a value of 8.7 cm$^{-1}$. From this series of spectra it can be concluded that only around half of the additional light absorbed in the PR composite is absorbed by the charge-generating species and the remainder is absorbed by the NPP.

For purposes of completeness, the photoconductive characteristics of the PVK:TCP:NPP:CdS were measured and are presented in Figure 8. As expected, this composite shows a dramatic decrease in photoconductivity compared to that of the PVK:CdS composite. This results from the significant dilution of charge carrier species, namely PVK, as well as the decrease in photons harvested by the charge-generating species as a result of the presence of NPP.

In addition to photoconductivity, effective electro-optic activity attributed to electronic ($\chi^3$) and/or birefringent (orientational) contributions must be simultaneously observed in a material in order for the possibility of photorefractive behavior to exist.[40] Due to the $C_{\infty v}$ symmetry of poled polymers, all electro-optic tensors vanish except those of $r_{13}$ and $r_{33}$. Figure 9 displays the dependence of the effective EO coefficients on the dc poling field at $\lambda = 514.5$ nm for the PVK:TCP:NPP:CdS composite as measured using the transmission configuration of the ellipsometric technique.[33] The data represented in Figure 9 were fitted to an equation of the form $y = (b)x^a$ using a least-squares method, giving values of $4.9 \times 10^{-2}$ and 0.97 for $b$ and $a$, respectively. Thus, the data indicate a sublinear increase with applied poling field, which is in accordance with the theoretically predicted electric field induced alignment of dipolar chromophores.[40]

While it is relatively easy to conduct, several disadvantages are associated with the ellipsometric technique: First, it allows for the determination of $|r_{33} - r_{13}|$. To separate these coefficients, one must make the assumption that $r_{33}/r_{13}$ is equal to 3 on the basis of a weak poling field.[30] Second, the measured effective EO coefficients include both electronic and orientational contributions. The Mach−Zender interferometric technique on the other hand, although tedious, permits a straightforward determination of $r_{33}$ and $r_{13}$. Also, by varying the frequency of the applied external ac field used in the

(40) Prasad, P. N.; Williams, D. J. *Introduction to Nonlinear Optical Effects in Polymers and Molecules*; Wiley: New York, 1991.

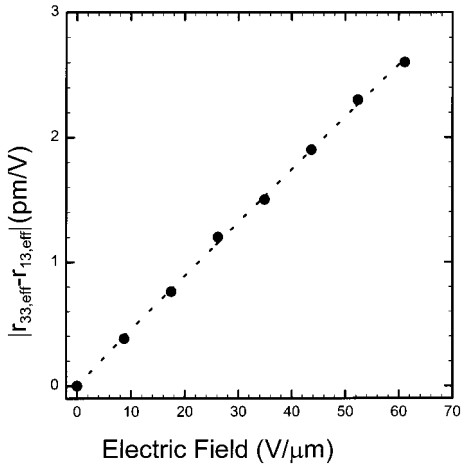


**Figure 9.** Electric field dependence of the effective electro-optic coefficients $|r_{33} - r_{13}|$ of the PVK:TCP:NPP:CdS ($S^{2-}$:$RS^{-}$ = 1:0.2) measured at 514.5 nm. The line represents $y = (4.88 \times 10^{-2})x^{0.9694}$ (see text).

performance of this experiment, it is possible to differentiate between the electronic and the birefringent contributions to the overall effective electro-optic coefficients. This is possible because at low frequencies the reorientation of the chromophores can completely follow the applied ac field. In this scenario the total possible contribution of the birefringence modulation together with the pure electronic contribution is measured. As the frequency of the applied ac field is increased, the chromophores are no longer able to reorient in response to the applied electric field, and as a result, only the pure electronic contribution is measured. The frequency dependences of the effective electro-optic coefficients $r_{33}$ and $r_{13}$ are presented in parts a and b of Figures 10, respectively. From these figures it can be concluded that, for frequencies below ~200 Hz, the measured refractive index modulation remains constant, indicating the chromophores are completely able to follow the modulating ac field. As the frequency is increased to ~1 kHz, a rapid decrease in the measured refractive index modulation is observed. Beyond this frequency the measured refractive index modulation again obtains a constant but significantly diminished value, representative of the pure electronic contribution. This indicates that the contribution to the refractive index modulation in the low-frequency range is predominantly from the reorientation of the linearly anisotropic chromophores (birefringence modulation). Consequently, the observed photorefractive effect associated with this composite can be attributed almost entirely to the orientational modulation of the birefringence.

A characteristic feature of the photorefractive effect is that the refractive index grating created in the medium is spatially shifted with respect to the light intensity pattern of the writing beams.[24,30] As a result an asymmetric energy transfer between beams interfering in a photorefractive sample occurs. Figure 11 depicts the data obtained in the TWM portion of the experiment to verify intensity exchange between laser beams and quantify the TWM gain coefficient for the PVK:TCP:NPP:CdS composite. For this experiment the writing beams, $I_1$ and $I_2$, with intensities of 227 and 83 mW/cm$^2$, respectively, were used while an external dc electric field $E_0$ = 107 V/$\mu$m was applied to a 168 $\mu$m thick sample at time $t$ = 70 s and turned off at $t$ = 190 s. A strongly biphasic nature of the data presented in Figure 11 is observed, suggesting the existence of two separate grating growth mechanisms. The involvement of two different charge carriers with varying generation efficiencies and/

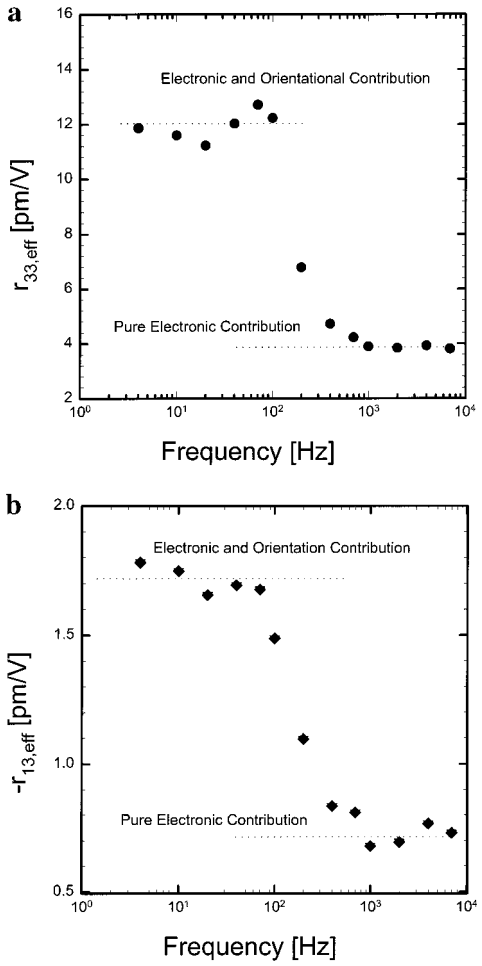


**Figure 10.** Frequency dependence of the effective electro-optic coefficients (a) $r_{33}$ and (b) $r_{13}$ at a poling field of 54 V/$\mu$m.

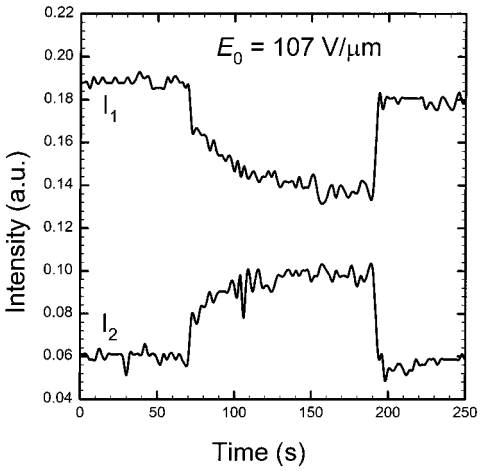


**Figure 11.** Example of asymmetric energy exchange between laser beams in the TWM experiment recorded at 514.5 nm in the PVK:TCP:NPP:CdS ($S^{2-}$:$RS^{-}$ = 1:0.2) composite. The external electric field was applied at $t$ = 70 s and turned off at $t$ = 190 s.

or mobilities offers one possible explanation and is the subject of current study.

The TWM coupling gain coefficient $\Gamma$ is given in terms of the experimentally measured quantities $\gamma_0$ and $\beta$ as

$$\Gamma = (1/L)[\ln(\gamma_0\beta) - \ln(\beta + 1 - \gamma_0)] \qquad (3)$$

where $L$ is the length of the optical path of the beam experi-

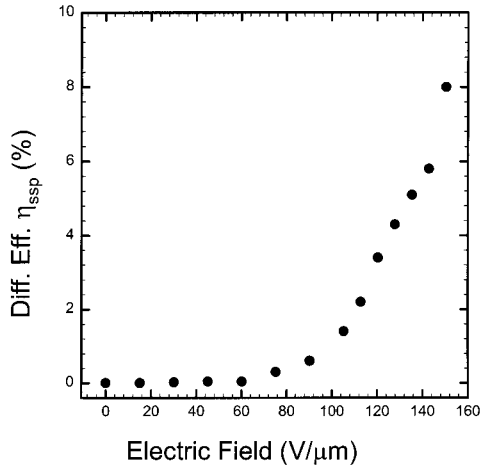


**Figure 12.** Dependence of steady-state diffraction efficiency in PVK:TCP:NPP:CdS ($S^{2-}$:$RS^{-}$ = 1:0.2) on electric field at 514.5 nm.

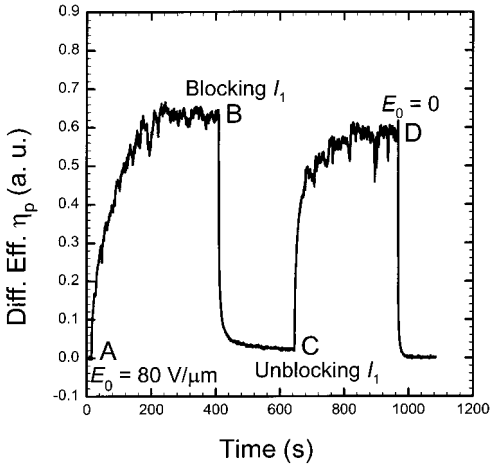


**Figure 13.** Temporal profile of diffraction efficiency of PVK:TCP:NPP:CdS ($S^{2-}$:$RS^{-}$ = 1:0.2) showing the following: point A, application of external electric field; B, blocking of writing beam $I_1$; C, unblocking of writing beam $I_1$; D, removal of external electric field.

encing gain inside the sample, $\beta$ is the ratio of the writing beam intensities before the sample, and $\gamma_0$ is the beam-coupling ratio, defined as

$$\gamma_0 = P_1/P_0 \tag{4}$$

where $P_1$ is the intensity of the signal with the pump and $P_0$ is the intensity of the signal without the pump.[18,24,30,40,42] A TWM gain coefficient of $\Gamma = 39.5$ cm$^{-1}$ for writing beams with p-polarization at 514.5 nm was calculated for the data depicted in the figure; however, it is noted that, when the sample was subjected to an external electric field of 119 V/$\mu$m, a TWM gain coefficient of $\Gamma = 59.5$ cm$^{-1}$ was measured just prior to the sample experiencing dielectric breakdown. From a practical point of view, the optical amplification, $\Gamma$, must exceed the absorption loss, $\alpha$, of the photorefractive sample in question.[24] In this case the optical absorption of the sandwiched sample (glass/ITO/polymer composite/ITO/glass) at 514.5 nm was measured to be $\alpha = 8.7$ cm$^{-1}$, yielding a net gain coefficient, $\Gamma - \alpha$, of 30.8 cm$^{-1}$ at 107 V/$\mu$m and 50.8 cm$^{-1}$ at 119 V/$\mu$m.

TWM characterizations were also performed using control samples which, aside from the fact that they contained no CdS, were otherwise identical to those used for data acquisition. These samples did not exhibited measurable asymmetric energy exchange.

In the DFWM experiment the writing beams, $I_1$ and $I_2$, were s-polarized and had intensities of 218 and 211 mW/cm$^2$, respectively. The reading beam, $I_r$, from the same $Ar^+$ ($\lambda$ = 514.5 nm) laser with p-polarization propagated in the direction opposite to $I_1$ with an intensity of 5.6 mW/cm$^2$. Given this geometry, the diffracted signal counterpropagated to $I_2$, where it was reflected by the beam splitter and detected by a photodetector. The electric field dependence of the photorefractive DFWM steady-state diffraction efficiency obtained in a sample with a thickness of 146 $\mu$m is presented in Figure 12. The maximum obtained steady-state diffraction efficiency, $\eta_{ssp}$, is 8% at $E_0 = 137$ V/$\mu$m. It is noted that the diffraction efficiency begins increasing rapidly only after $E_0$ has exceeded 80 V/$\mu$m.

Figure 13 shows the diffraction efficiency as a function of time with a sample thickness of 169 $\mu$m. Two writing beams are turned on at time $t = 0$, followed by the subsequent application of an external electric field ($E_0 = 80$ V/$\mu$m) at $t$ = 15 s depicted as point A in Figure 13, at which time a rapid rise in diffraction efficiency is observed. At the point depicted as point B ($t = 408.5$ s) in Figure 13, the writing beam $I_1$ is blocked, which results in relatively uniform illumination of the sample, leading to the erasure of the photorefractive grating. This ultimately causes a rapid decrease in the diffraction efficiency. At point C ($t = 646$ s) the blocked writing beam, $I_1$, is unblocked, allowing the PR grating to again achieve a steady state. At point D ($t = 968$ s) the external electric field is turned off, which allows for the random reorientation of the chromophores, leading to the erasure of the PR grating. The characteristic growth time, $\tau$, can be determined using the equation

$$\eta_p(t) \approx [E_{sc}(1 - e^{-t/\tau})]^2 \tag{5}$$

where $E_{sc}$ is the saturation value of the space-charge field.[21] A value of $\tau = 7.3$ s was calculated for the sample by fitting the data represented between points C and D in Figure 13 to eq 5.

In addition to demonstrating the temporal characteristics of the photorefractive grating written in this composite, this figure also serves to illustrate the possibility of recording and erasing PR gratings repeatedly in this composite.

## Conclusions

The ability to use semiconductor nanoparticles as a photoconductive sensitizer in a PVK matrix as well as the ability to control the optical properties of these particles to suit the required needs of the composite has been demonstrated. While the photoconductivity observed in the PVK:CdS composites is comparable to values reported for PVK:$C_{60}$ systems, the photorefractive properties of the PVK:TCP:NPP:CdS composite are lower than those reported for similar materials utilizing $C_{60}$ as the sensitizer.[24,30] The increase in photoconductivity is probably due to the ability to achieve relatively higher loading for encapsulated CdS as opposed to $C_{60}$ (>1% for CdS compared with 0.2% for $C_{60}$).[43] Several factors may lead to the diminished photorefractive behavior of the CdS-doped composite, including the higher dielectric constant associated with inorganic materials. This increase in dielectric constant leads to a decrease in the effective space-charge field experienced by the chromophores. Also, it has been shown that the addition of $C_{60}$ to polymeric composites not only leads to an increase in

(41) Yeh, P. *IEEE J. Quantum Electron.* **1989**, *25*, 484.
(42) Donckers, M. C. J. M.; Silence, S. M.; Walsh, C. A.; Hache, F.; Burland, D. M.; Moerner, W. E.; Tweig, R. J. *Opt. Lett.* **1993**, *18*, 1044.
(43) Silence, S. M.; Walsh, C. A.; Scott, J. C.; Moerner, W. E. *Appl. Phys. Lett.* **1992**, *61*, 2967−2969.

absorption coefficient of these composites at the operating wavelength but also increases the quantum efficiency and density of shallow traps.[43] The ability, or lack thereof, of CdS to perform these functions is under current investigation.

It is also noted that the photorefractive characterization of this composite was carried out at 514.5 nm, chosen because it lies just outside the low-energy absorption edge of the nonlinear dye, NPP. However, an increase in the photorefractive figures of merit is anticipated at shorter wavelengths where the absorption coefficient of nanoparticle CdS is significantly higher. Alternative nonlinear dyes which would allow for the realization of these studies are currently being sought. Also, other semiconductor nanoparticles which retain the exceptional sensitizing abilities of CdS and furthermore possess a smaller intrinsic band gap, extending the useful range of the sensitizer farther into the red portion of the visible spectrum, are under current investigation.

**Acknowledgment.** We acknowledge Dr. S. Goshal of Laser Photonics Technology, Inc., for providing us with NPP, K. Kim for his suggestion of an appropriate capping reagent, and especially Dr. R Burzynski of Laser Photonics Technology, Inc., for his thorough review of this manuscript. This work was supported in part by the Directorate of Chemistry and Life Sciences of the Air Force Office of Scientific Research (Contract No. F496209610124) and in part by the MURI program through the University of Southern California (Primary Contract Number 000507).

JA983559W